This is the accepted version of the work. The final published article is available at https://doi.org/10.1139/cgj-2018-0409

Bayesian updating of subsurface spatial variability for improved prediction of braced excavation response

M.K. Lo and Y.F. Leung*

Department of Civil and Environmental Engineering, The Hong Kong Polytechnic University
*Corresponding author, email address: andy.yf.leung@polyu.edu.hk

Abstract

This paper introduces an approach that utilizes field measurements to update the parameters characterizing spatial variability of soil properties and model bias, leading to refined predictions for subsequent construction stages. It incorporates random field simulations and surrogate modeling technique into the Bayesian updating framework, while the spatial and stage-dependent correlations of model bias can also be considered. The approach is illustrated using two cases of multi-stage braced excavations, one being a hypothetical scenario and the other from a case study in Hong Kong. Making use of all the deflection measurements along an inclinometer, the principal components of the random field and model bias factors can be efficiently updated as the instrumentation data becomes available. These various sources of uncertainty do not only cause discrepancies between prior predictions and actual performance, but can also lead to response mechanisms that cannot be captured by deterministic approaches, such as distortion of the wall along the longitudinal direction of the excavation. The proposed approach addresses these issues in an efficient manner, producing prediction intervals that reasonably encapsulate the response uncertainty as shown in the two cases. The capability to continuously refine the response estimates and prediction intervals can help support the decision-making process as the construction progresses.

Keywords: Bayesian updating, braced excavations, soil-structure interaction, spatial variability, random field modeling

Introduction

In many geotechnical engineering projects, predictions of system performance at the design stage can deviate from actual site response during construction, due to various sources of geotechnical uncertainty, such as inherent spatial variations of soil properties or model uncertainty (e.g., Phoon and Kulhawy 1999; Baecher and Christian 2003). The observational method, as outlined by Peck (1969), emphasizes the needs to incorporate new knowledge of site conditions as construction progresses and, if necessary, revise the original assumptions during the process. This is particularly important for deep excavation projects in the urban areas, where geotechnical failures can lead to catastrophic results. Meanwhile, the multiple stages of shoring installation in these projects offer opportunities for fine adjustments of the support layout if such needs are revealed from the monitoring data. In order to achieve this, an efficient and reliable analysis technique is required to rationally incorporate the knowledge gained from the data, and reflect that onto refined predictions for subsequent stages.

The Bayesian approach provides a quantitative framework by which initial assumptions on material property (prior probability) are updated, through subsequent observations, to obtain the posterior probability. Bayesian methods have been applied in various aspects of geotechnical engineering, including site characterization (e.g., Zhang et al. 2009; Ching et al. 2010; Wang et al. 2010, 2014, 2016; Huang et al. 2018) and soil-structure interaction problems (e.g., Ledesma et al. 1996; Najjar and Gilbert 2009; Zhang et al. 2012; Lo and Leung 2016). For deep excavations, stepwise updating of predictions for retaining wall response can be tackled by Bayesian methods (e.g., Papaioannou and Straub 2012; Juang et al. 2013; Wu et al. 2014; Qi and Zhou 2017), or other techniques such as the artificial neural network (ANN) approach (e.g., Jan et al. 2002; Kung et al. 2007) and inverse analyses coupled with optimization algorithms (e.g., Finno and Calvello 2005; Baroth and Malecot 2010). In these previous studies, however, soil properties are considered to be homogeneous within each soil layer, where spatial variability is not explicitly accounted for. This may be attributed to the computational demands associated with modeling of soil spatial variability, which can be exacerbated when incorporated into an updating framework, such as the updating of posterior probability for random field parameters. Nonetheless, probabilistic analyses in recent studies (e.g., Sert et al. 2016; Yáñez-Godoy et al. 2017) have shown that spatial variability can have significant implications on the response of retaining structures, although there has been limited discussion on the integration of random field theories into the updating framework for improved predictions of system response.

Lo and Leung (2016) presented a Bayesian approach to update spatial variability parameters for soils below building foundations, but their approach required a large number of model simulations. Later, Yang et al. (2018) utilized surrogate modeling techniques to reduce the computational demands for random field analyses of slopes, where the spatial variability in soil permeability were back-analyzed with field observations. This study further extends the Bayesian framework for applications in multi-stage deep excavations, where the characteristics of the random field of soil properties are 'indirectly' conditioned using measurements of wall deflections. It differs from previous studies of Bayesian methods as the spatial variation patterns of the soils are explicitly considered using surrogate modeling technique, and are updated through field measurements. Moreover, the subsurface model is not only 'back-calibrated' as in Yang et al. (2018), but allows wall deflections to be continuously refined for subsequent excavation stages. As a key component in the updating process, the model uncertainty is also assumed to be spatially correlated, and the correlation features (e.g., mean, variance, autocorrelation distance) are not pre-specified, but determined directly using field measurements. The concept of stage-wise correlation in model uncertainty is also explored, through which the observed model bias in the current construction stage can be utilized to predict that in the next stage. The proposed framework aims to maximize the value of instrumentation in deep excavation projects, by integrating the evaluation of soil spatial variability and model uncertainty, with continuous refinement of response prediction during the multi-stage construction process. The integration of these new features allows the proposed approach to serve as a quantitative tool for the observational method. The following sections introduce the formulation of the proposed approach, while the implementation and its validity are illustrated first through a hypothetical excavation scenario, and then by an instrumented case study of a deep excavation project in Hong Kong.

Formulation of updating approach

Probabilistic modeling of braced excavations in spatially variable soils

Performance of retaining structure in a deep excavation involves complex soil-structure interaction effects, and the reliability of such systems may be evaluated using probabilistic methods. In this study, two major factors affecting the uncertainty of wall deflections are investigated, namely the spatial variations in soil strength and stiffness, and the model uncertainty/bias involved in the numerical simulations. Due to their influences, the measured wall response (represented by $\boldsymbol{y}$) often show discrepancies from the prediction ($\boldsymbol{g}$). Such discrepancies are considered holistically in the proposed approach: the spatial correlations in soil properties are modeled by random field theory using surrogate modeling technique, while the model uncertainty is represented by bias factors, and both the principal components of the random field and model bias factors are updated and refined using field measurements as the construction progresses.

In many deep excavation projects, inclinometer measurements are either taken within the retaining structure (e.g., diaphragm wall) or immediately behind, so that its performance during the construction are closely monitored. In this study, the inclinometer measurements are denoted by the vector $\boldsymbol{y} = \{y_1, y_2, \ldots, y_n\}$, which represent the actual deflections at different depths ($k = 1, 2, \ldots, n$) along the retaining wall. The corresponding predictions of wall deflections are represented by vector $\boldsymbol{g} = \{g_1, g_2, \ldots, g_n\}$, while the predicted and actual deflections are linked by a model bias term $\boldsymbol{\varepsilon}$:

$$\boldsymbol{y} = \boldsymbol{\varepsilon} \cdot \boldsymbol{g}(\boldsymbol{\xi}) \tag{1}$$

and the bias at different depths (ε_k) may vary. In equation (1), the predicted response $\boldsymbol{g}$ can be represented as a function of $\boldsymbol{\xi}$ vectors, which are standard normal random variables that characterize the spatially variable soil properties $\boldsymbol{z}$. In this study, variations of $\boldsymbol{z}$ in three dimensions are considered, and modeled as the combination of a trend with different values of residuals, or deviations from the trend. For residuals that are correlated spatially, and assuming a squared exponential autocorrelation function, the spatial correlation matrix ($\mathbf{R}$) consists of the following components:

$$R_{ij} = \exp\left[-\frac{(x_i - x_j)^2}{\theta_x^2} - \frac{(y_i - y_j)^2}{\theta_y^2} - \frac{(z_i - z_j)^2}{\theta_z^2}\right] \tag{2}$$

where x, y and z represent the Cartesian coordinates at locations i and j; θ_x, θ_y and θ_z are the corresponding autocorrelation distances. Although this study adopts the squared exponential function for $\mathbf{R}$, the proposed approach is not confined to this assumption, as it is also possible to assume the single exponential function, or even Matérn function (Liu et al. 2017) for $\mathbf{R}$. As will be shown in a later example, the more fundamental issue is the estimation of relevant parameters (e.g., θ) that correspond to the adopted functional form, using site-specific geotechnical data.

A spectral decomposition of the $\mathbf{R}$ matrix can be performed, i.e.,$\mathbf{R} = \mathbf{H}\boldsymbol{\Lambda}\mathbf{H}^T$, where $\mathbf{H}$ is a matrix of orthonormal eigenvectors, and $\boldsymbol{\Lambda}$ is a diagonal matrix of positive descending eigenvalues. Denoting $\mathbf{H}^* = \mathbf{H}\boldsymbol{\Lambda}^{\frac{1}{2}}$, realizations of $\boldsymbol{z}$ profiles can then be generated using the $\boldsymbol{\xi}$ vectors (Lo and Leung 2018):

$$\boldsymbol{z} = \begin{cases} \boldsymbol{\mu}_{\boldsymbol{z}} + \sigma_{\boldsymbol{z}}\mathbf{H}^*\boldsymbol{\xi} & \text{for normal random field} \\ \exp\left(\boldsymbol{\mu}_{\ln \boldsymbol{z}} + \sigma_{\ln \boldsymbol{z}}\mathbf{H}^*\boldsymbol{\xi}\right) & \text{for lognormal random field} \end{cases} \tag{3}$$

where $\boldsymbol{\mu}$ and σ represent the mean (or trend) vector and standard deviation of the soil properties, and the subscripts $\boldsymbol{z}$ or $\ln \boldsymbol{z}$ correspond to the original space (normal distribution) or log space (lognormal distribution), respectively. For soil data that involves a clear trend (e.g., undrained shear strength increasing with depth), the trend can be determined by regression and is represented by $\boldsymbol{\mu}$, while the random field simulation involves random variables that are only associated with the residuals, represented by the second term in equation (3). This term also implies that each component of $\boldsymbol{\xi}$ (e.g., ξ_i) corresponds to a different variation pattern associated with the i^{th} column of $\mathbf{H}^*$. The first few components of $\boldsymbol{\xi}$ determine the large-scale variations, while the latter ones correspond to small-scale variations or rapid changes across space. A similar concept was presented graphically by Yang et al. (2018), who illustrated the various components in Karhunen-Loève expansion of the spatially variable field.

A number of realizations are required to envelope the potential variations of subsurface soil properties. Conventionally, the various realizations are then evaluated using finite element or finite difference methods. However, these numerical methods are usually computationally demanding, which poses a substantial obstacle for Bayesian updating, as random field modeling is required at every stage of the construction process. To reduce the computational demands, this study adopts a response surface method known as the polynomial chaos expansion (PCE)(Ghanem and Spanos 1991; Al-Bittar and Soubra 2014). At a certain depth k, the response (wall deflection) g_k may be approximated using a second-order PCE as follows:

$$g_k(\boldsymbol{\xi}) = a_{k,0} + \sum_{j=1}^{M} a_{k,j}\xi_j + \sum_{j_1=1}^{M}\sum_{j_2=j_1}^{M} a_{k,j_1,j_2}(\xi_{j_1}\xi_{j_2} - \delta_{j_1 j_2}) \tag{4}$$

where $k = 1, 2, \ldots, n$ may represent different depths along the wall; $a_{k,0}$, $a_{k,j}$ and a_{k,j_1,j_2} are coefficients of the PCE, to be determined by the regression approach using results from random field simulations. M is the number of principal components retained in the PCE, which will be elaborated later. The mathematical details and implementation of PCE are not described herein, as they have been reported extensively in several previous studies including Ghanem and Spanos (1991), Blatman and Sudret (2010), Al-Bittar and Soubra (2014) and Lo and Leung (2017), the latter of which also combined PCE with a stratified sampling technique known as Latin hypercube sampling with dependence (LHSD)(Packham and Schmidt 2010), in order to enhance the robustness of probabilistic analyses. In the current formulation, a separate PCE is constructed for each location k along the depth of the wall. For example, inclinometer readings are often taken at vertical interval of 0.5 m. While each reading will constitute a component (y_k) in the $\boldsymbol{y}$ vector, the corresponding prediction is represented by g_k, and the two are linked to each other through a multiplicative error term, ε_k, in equation (1).

In general, M should be equal to the total number of random variables, i.e., the number of elements in the finite element mesh (d). Alternatively, this can be truncated by considering only the principal components that contribute to most (e.g., 95%) of the total variance of the random field:

$$\min_{M} \sum_{i=1}^{M} \lambda_i > 0.95d \tag{5}$$

where λ_i are the eigenvalues from the $\mathbf{\Lambda}$ matrix. From the spectral decomposition of $\mathbf{R}$, λ_i decreases monotonically ($\lambda_1 > \lambda_2 > \cdots > \lambda_M$), so does the influence of the corresponding ξ_i components to the random field. With the truncation of equation (5), the dimension of $\boldsymbol{\xi}$ can still be too large for direct application in the Bayesian framework. To further enhance the robustness of the updating algorithm, only the ξ components which are most influential to the wall deflection response should be updated. This can be assessed using a sensitivity index, and this study adopts the first-order Sobol' index, $S_k(\xi_i)$, which quantifies the contribution of component ξ_i to the overall variance of response g_k. Applying the first-order Sobol' index evaluation to a second-order PCE (Al-Bittar and Soubra 2014) yields

$$S_k(\xi_i) = \frac{a_{k,i}^2 + 2a_{k,ii}^2}{\mathrm{Var}(g_k)} \tag{6}$$

which does not consider the cross-terms (a_{k,j_1j_2} where $j_1 \neq j_2$). Because of this, the S_k values do not add up to unity ($\sum_i S_k(\xi_i) < 1$), making it inconvenient when comparing influence of ξ_i components across different depths k. Therefore, a different formulation is adopted in this study to take into consideration the influence of cross-terms:

$$S_k(\xi_i) = \frac{a_{k,i}^2 + 2a_{k,ii}^2 + 0.5\left(\sum_{j_1=1}^{i-1} a_{k,j_1i}^2 + \sum_{j_2=i+1}^{M} a_{k,ij_2}^2\right)}{\mathrm{Var}(g_k)} \tag{7}$$

which ensures the sum of $S_k(\xi_i)$ values become unity. In the subsequent Bayesian updating process, only the ξ_i components with the highest Sobol' index values are selected for updating. In this study, p components are included such that their sum encapsulates the majority of variance contribution to the deflection response along the wall. For example, to incorporate 90% of variance contribution to the response, $\sum_{k=1}^{n} \sum_p S_k(\xi_p) > 0.9n$. This procedure further reduces the number of principal components required in the representation of the response $\boldsymbol{g}$ by PCE (equation(4)), and the subsequent Bayesian updating algorithm.

Bayesian updating with spatially-correlated soils and model uncertainty

Following the preceding description of probabilistic approach, the main objectives of Bayesian analyses involve updating the ξ components and the model bias ($\boldsymbol{\varepsilon}$) through site measurements $\boldsymbol{y}$. Based on comparisons between predicted and measured displacements at 49 wall sections from 11 case studies, Qi and Zhou (2017) noted that, in general, the values of $\boldsymbol{\varepsilon}$ are similar at measurement points that are close to each other, which is another manifestation of spatial correlation. They also noted that $\boldsymbol{\varepsilon}$ broadly follows lognormal distributions and, consequently, established the correlation matrix for model bias factors at different separation distances between measurement points. In this study, the correlation structure of model bias is represented by an $n \times n$ $\mathbf{C}_{\ln \varepsilon}$ matrix, with components assumed to follow a squared exponential function:

$$(C_{\ln \varepsilon})_{ij} = \sigma^2_{\ln \varepsilon} \exp\left[-\frac{(\Delta D_{\mathrm{v}}/H)^2}{(\theta_{\mathrm{spv}})^2}\right] \tag{8}$$

where ΔD_{v} is the vertical separation distance between two inclinometer measurement points i and j, and H is the final excavation depth; $\sigma_{\ln \varepsilon}$ and θ_{spv} represent the standard deviation and vertical autocorrelation distance (normalized by H) of the model bias. Equation (8) is conceptually similar to the recommendations by Qi and Zhou (2017), although they normalized ΔD_{v} and autocorrelation distance with the excavation depth at the current stage, and proposed constant values for the spatial correlations. Since constant spatial correlations may not apply equally well to the large varieties of site settings or different soil constitutive relations in the numerical model, this study proposes a more general approach, where distributions of σ_ε, θ_{spv} and μ_ε (mean bias) are refined through site measurements within the Bayesian framework, and σ_ε and μ_ε can be converted to $\sigma_{\ln \varepsilon}$ and $\mu_{\ln \varepsilon}$ through the relationships between lognormal and normal distribution parameters.

Where multiple inclinometers are installed along the lateral directions of retaining structure, equation (8) may be extended to consider also the correlation of $\boldsymbol{\varepsilon}$ in horizontal directions:

$$(C_{\ln\varepsilon})_{ij} = \sigma^2_{\ln\varepsilon} \exp\left[-\frac{(\Delta D_{\mathrm{v}}/H)^2}{(\theta_{\mathrm{spv}})^2} - \frac{(\Delta D_{\mathrm{h}}/H)^2}{(\theta_{\mathrm{sph}})^2}\right] \tag{9}$$

where ΔD_{h} is the horizontal separation distance between measurement points and θ_{sph} is the horizontal autocorrelation distance of model bias, normalized by H.

In this study, the model bias is assumed to be stationary with a mean value of μ_ε and standard deviation of σ_ε. These values can also be updated by the Bayesian approach, which means there can be prior distributions of μ_ε and σ_ε. Their prior (and posterior) distributions are characterized by a mean ($m_{\mu\varepsilon}$ and $m_{\sigma\varepsilon}$) and a standard deviation ($s_{\mu\varepsilon}$ and $s_{\sigma\varepsilon}$). Similarly, $m_{\theta\mathrm{sp}}$ and $s_{\theta\mathrm{sp}}$ describe the distributions of autocorrelation distance of $\boldsymbol{\varepsilon}$, and may represent the vertical and/or horizontal directions. Therefore, the prior distributions for spatial correlation parameters of model bias, represented in logarithmic space, are given by:

$$\ln f(\mu_\varepsilon) = \mathrm{const} - \frac{(\mu_\varepsilon - m_{\mu\varepsilon})^2}{2s^2_{\mu\varepsilon}} \tag{10a}$$

$$\ln f(\sigma_\varepsilon) = \mathrm{const} - \frac{(\sigma_\varepsilon - m_{\sigma\varepsilon})^2}{2s^2_{\sigma\varepsilon}} \tag{10b}$$

$$\ln f(\theta_{\mathrm{sp}}) = \mathrm{const} - \frac{(\theta_{\mathrm{sp}} - m_{\theta\mathrm{sp}})^2}{2s^2_{\theta\mathrm{sp}}} \tag{10c}$$

where 'const' denotes the normalizing constant for the probability density function. The prior distribution for soil profiles, represented by the $\boldsymbol{\xi}$ vectors, is given as follows:

$$\ln f(\boldsymbol{\xi}) = \mathrm{const} - \frac{1}{2}\ln|\mathbf{C}_{\boldsymbol{\xi}}| - \frac{1}{2}(\boldsymbol{\xi} - \boldsymbol{\mu}_{\boldsymbol{\xi}})^T \mathbf{C}_{\boldsymbol{\xi}}^{-1}(\boldsymbol{\xi} - \boldsymbol{\mu}_{\boldsymbol{\xi}}) \tag{11}$$

where $\boldsymbol{\mu}_{\boldsymbol{\xi}}$ and $\mathbf{C}_{\boldsymbol{\xi}}$ represent the mean vector and covariance matrix of the ξ components, respectively. In the first stage, $\boldsymbol{\mu}_{\boldsymbol{\xi}}$ is a zero vector and $\mathbf{C}_{\boldsymbol{\xi}}$ is an identity matrix as $\boldsymbol{\xi}$ are independent standard normal vectors. During the updating process, $\boldsymbol{\mu}_{\boldsymbol{\xi}}$ and $\mathbf{C}_{\boldsymbol{\xi}}$ will be evaluated with the Markov Chain Monte Carlo (MCMC) procedure, which will be elaborated later.

At a certain construction stage, inclinometer measurements $\boldsymbol{y}$ become available. Considering the logarithm of equation (1): $\ln \boldsymbol{\varepsilon} = \ln \boldsymbol{y} - \ln \boldsymbol{g}(\boldsymbol{\xi})$, the log-likelihood function for soil profile $\boldsymbol{\xi}$, given data $\boldsymbol{y}$, is related to the distribution of model uncertainty, $\ln \boldsymbol{\varepsilon}$, which is multivariate normal. The log-likelihood function then becomes:

$$L(\boldsymbol{\xi}|\boldsymbol{y}) = \text{const} - \frac{1}{2}\ln|\mathbf{C}_{\ln\varepsilon}| - \frac{1}{2}(\ln\boldsymbol{\varepsilon} - \boldsymbol{\mu}_{\ln\varepsilon})^T \mathbf{C}_{\ln\varepsilon}^{-1}(\ln\boldsymbol{\varepsilon} - \boldsymbol{\mu}_{\ln\varepsilon}) \tag{12}$$

and $\boldsymbol{\mu}_{\ln\varepsilon}$ is a constant vector since $\boldsymbol{\varepsilon}$ is stationary. According to the Bayes' theorem, the posterior distribution of soil profile and model bias is the product of likelihood function and prior distributions (Ledesma et al. 1996). Represented in logarithmic space, this becomes:

$$\ln f(\boldsymbol{\xi}, \mu_\varepsilon, \sigma_\varepsilon, \theta_{\text{sp}}|\boldsymbol{y}) = \text{const} + L(\boldsymbol{\xi}|\boldsymbol{y}) + \ln f(\boldsymbol{\xi}) + \ln f(\mu_\varepsilon) + \ln f(\sigma_\varepsilon) + \ln f(\theta_{\text{sp}}) \tag{13}$$

Sampling of the posterior distribution is performed by the MCMC method, which has been described in detail by Juang et al. (2013). In short, the Markov chain sample at the current chain length is denoted as $\boldsymbol{x}_t$, with a length of $(p+3)$ or $(p+4)$, which includes p selected ξ components with 3 or 4 model bias parameters. A proposed Markov Chain sample is then generated based on the current sample $\boldsymbol{x}_t$ and the proposal distribution, which is multivariate normal with covariance matrix $\mathbf{C}_t$. The proposed Markov Chain sample is evaluated by equation (13) to obtain the posterior density, which is compared with that of the current sample to decide if the proposed sample would be accepted. In this study, the posterior distribution is high-dimensional ($p+3$ or $p+4$), the acceptance rate tends to be low if the proposal covariance is not modified during MCMC sampling. To this end, a specific type of MCMC known as adaptive metropolis (AM) algorithm (Haario et al. 2001) is adopted: if the current chain length t is larger than the initial chain length t_0, the proposal covariance $\mathbf{C}_t$ is built from the empirical covariance of previous MCMC samples $\boldsymbol{x}_0, \ldots, \boldsymbol{x}_t$:

$$\mathbf{C}_t = \begin{cases} \mathbf{C}_0 & \text{for } t \leq t_0 \\ s_\mathrm{d}\ \mathrm{Cov}(\boldsymbol{x}_0, \ldots, \boldsymbol{x}_t) + 0.001 s_\mathrm{d}\mathbf{I} & \text{for } t > t_0 \end{cases}$$
$$\text{where} \qquad \mathbf{C}_0 = s_\mathrm{d} \begin{pmatrix} \mathbf{C}_\xi & 0 & 0 & 0 \\ 0 & s^2_{\mu\varepsilon} & 0 & 0 \\ 0 & 0 & s^2_{\sigma\varepsilon} & 0 \\ 0 & 0 & 0 & s^2_{\theta\mathrm{sp}} \end{pmatrix} \tag{14}$$

where $s_\mathrm{d} = 2.4^2/(p+3)$ or $2.4^2/(p+4)$, and is a scaling parameter suggested by Gelman et al. (1996); $\mathbf{I}$ is the identity matrix and a small number is added to the diagonal through the second term, to ensure $\mathbf{C}_t$ will not become singular. The initial proposal distribution $\mathbf{C}_0$ is a scaled prior covariance matrix. As the Markov Chain grows longer, calculating $\mathbf{C}_t$ using equation (14) at each chain length will cost enormous computational time. To avoid this, Haario et al. (2001) proposed a recursive relationship to calculate $\mathbf{C}_t$ directly from $\mathbf{C}_{(t-1)}$, which is also adopted herein. Once the MCMC sampling is complete, the mean and covariance of the posterior distribution is estimated as the empirical mean and covariance of the Markov chain.

As will be shown in the later case studies, the number of variables to be updated is around 10. For this medium number of variables, the AM algorithm can converge satisfactorily to the posterior distribution with acceptance rate of around 50% to 60%. With larger number of variables to be updated (e.g., around 30), the use of advanced MCMC algorithms such as Metropolis within Gibbs (Juang and Zhang 2017) is recommended to improve convergence of the algorithm.

The posterior distribution of $\boldsymbol{\xi}$ (i.e., $\boldsymbol{\xi}|\boldsymbol{y}$) can be converted back to the posterior distribution of the actual soil profile $\boldsymbol{z}$ (i.e., $\boldsymbol{z}|\boldsymbol{y}$), by considering the transformation shown in equation (3). For a normal random field of $\boldsymbol{z}$:

$$\mathrm{E}(\boldsymbol{z}|\boldsymbol{y}) = \boldsymbol{\mu}_{\boldsymbol{z}} + \sigma_{\boldsymbol{z}}\mathbf{H}^{*}\mathrm{E}(\boldsymbol{\xi}|\boldsymbol{y}) \tag{15a}$$

$$\mathrm{Var}(\boldsymbol{z}|\boldsymbol{y}) = \sigma_{\boldsymbol{z}}^{2}\ \mathrm{Diag}\left[\mathbf{H}^{*}\mathrm{Cov}(\boldsymbol{\xi}|\boldsymbol{y})\mathbf{H}^{*T}\right] \tag{15b}$$

In equation (15)(b), the variance of $\boldsymbol{z}$, given $\boldsymbol{y}$, is obtained from $\mathbf{H}^{*}$ and covariance of $\boldsymbol{\xi}|\boldsymbol{y}$ (Anderson 1984). If the random field of $\boldsymbol{z}$ is lognormal, $\mathrm{E}(\ln \boldsymbol{z}|\boldsymbol{y})$ and $\mathrm{Var}(\ln \boldsymbol{z}|\boldsymbol{y})$ can be first calculated using similar equation forms as in equation (15), replacing $\boldsymbol{\mu}_{\boldsymbol{z}}$ and $\sigma_{\ln \boldsymbol{z}}$ by $\boldsymbol{\mu}_{\ln \boldsymbol{z}}$ and $\sigma_{\ln \boldsymbol{z}}$. The mean and variance can then be converted back to original space by:

$$\mathrm{E}(\boldsymbol{z}|\boldsymbol{y}) = \exp[\mathrm{E}(\ln \boldsymbol{z}|\boldsymbol{y}) + 0.5\mathrm{Var}(\ln \boldsymbol{z}|\boldsymbol{y})] \tag{16a}$$

$$\mathrm{Var}(\boldsymbol{z}|\boldsymbol{y}) = \mathrm{E}(\boldsymbol{z}|\boldsymbol{y})^{2}\{\exp[\mathrm{Var}(\ln \boldsymbol{z}|\boldsymbol{y})] - 1\} \tag{16b}$$

Based on the posterior estimates of soil properties and model uncertainty, predictions of wall deflections can be made for future construction stages. The variable to be predicted is denoted as $\boldsymbol{y}^{*}|\boldsymbol{y}$, which means the deflection of a future construction stage, conditional on the deflection of current stage. The prediction interval of $\boldsymbol{y}^{*}|\boldsymbol{y}$ is defined herein as conditional mean plus and minus one conditional standard deviation, i.e. $\mathrm{E}(\boldsymbol{y}^{*}|\boldsymbol{y}) \pm \mathrm{SD}(\boldsymbol{y}^{*}|\boldsymbol{y})$. Meanwhile, $\boldsymbol{y}^{*}|\boldsymbol{y}$ should incorporate both model uncertainty $\boldsymbol{\varepsilon}|\boldsymbol{y}$ and soil variability $\boldsymbol{\xi}|\boldsymbol{y}$, the latter of which is reflected in the model prediction $\boldsymbol{g}^{*}|\boldsymbol{y}$. Assuming these two components to be independent of each other, $\mathrm{E}(\boldsymbol{y}^{*}|\boldsymbol{y})$ and $\mathrm{SD}(\boldsymbol{y}^{*}|\boldsymbol{y})$ are evaluated from the product of two independent variables $\boldsymbol{\varepsilon}|\boldsymbol{y}$ and $\boldsymbol{g}^{*}|\boldsymbol{y}$:

$$\mathrm{E}(\boldsymbol{y}^*|\boldsymbol{y}) = \mathrm{E}(\mu_\varepsilon|\boldsymbol{y})\mathrm{E}(\boldsymbol{g}^*|\boldsymbol{y}) \tag{17a}$$

$$\mathrm{SD}(\boldsymbol{y}^*|\boldsymbol{y}) = \sqrt{\mathrm{E}(\sigma_\varepsilon|\boldsymbol{y})^2\mathrm{Var}(\boldsymbol{g}^*|\boldsymbol{y}) + \mathrm{E}(\sigma_\varepsilon|\boldsymbol{y})^2\mathrm{E}(\boldsymbol{g}^*|\boldsymbol{y})^2 + \mathrm{Var}(\boldsymbol{g}^*|\boldsymbol{y})\mathrm{E}(\mu_\varepsilon|\boldsymbol{y})^2} \tag{17b}$$

where $\mathrm{E}(\mu_\varepsilon|\boldsymbol{y})$ and $\mathrm{E}(\sigma_\varepsilon|\boldsymbol{y})$ are the posterior mean of the parameters μ_ε and σ_ε, estimated from the Markov Chain.

Instead of conducting a large number of random field simulations to determine $\mathrm{E}(\boldsymbol{g}^*|\boldsymbol{y})$ and $\mathrm{Var}(\boldsymbol{g}^*|\boldsymbol{y})$ at each of the updating stages, this study proposes to evaluate them using the PCE surrogate model, which is computationally more efficient. A large number of $\boldsymbol{\xi}|\boldsymbol{y}$ are simulated through the mean and covariance of posterior distribution, obtained from MCMC. These are evaluated by the surrogate model (equation (4)) to obtain the posterior model prediction $\boldsymbol{g}^*|\boldsymbol{y}$. Through the use of surrogate model, it is not necessary to perform random field simulations during each construction stage. Only a single set of simulation is necessary to construct the PCE that represent the response in all stages, through which the predictions can be obtained directly. The implementation will be illustrated by two examples in later sections.

Stage correlation of model uncertainty

While the preceding formulation describes spatial features of soil variability and model bias, 'stage-dependent' correlations may also exist between model bias: if a prediction model overestimates the actual response in construction stage 1, it is also likely to overestimate the response in stage 2, and so on. This aspect of model uncertainty had been investigated by Wu et al. (2014), who developed a regression model for maximum wall deflections for excavations in soft clay, based on 35 sets of inclinometer readings from 22 case histories. They found that the bias in the regression model are positively-correlated between construction stages, and they defined a 'correlation length' which was estimated to be 23 m. This correlation length is conceptually similar to the idea of autocorrelation distance that is associated with differences in excavation depths at various stages. This term will be denoted as 'stage autocorrelation distance' in this study, represented by θ_{st}.

The updating approach in this study can be extended to incorporate this stage correlation in model bias, which further refines the prediction interval of wall deflections. While the model bias for the current stage is represented by $\boldsymbol{\varepsilon}$, the predicted bias for the next stage may be denoted as $\boldsymbol{\varepsilon}^*$. Wu et al. (2014) adopted an exponential function to represent the stage correlation for maximum wall deflection. Assuming this is also valid for stage correlation between ε_k and ε_k^* (at the same location), the $n \times n$ cross-covariance matrix between model bias in two construction stages can be constructed by modifying equation (8):

$$\mathbf{C}_{\ln \boldsymbol{\varepsilon}, \ln \boldsymbol{\varepsilon}^*} = \rho \mathbf{C}_{\ln \varepsilon} = \mathbf{C}_{\ln \varepsilon} \exp\left[-\frac{\Delta D_{\mathrm{st}}}{\theta_{\mathrm{st}}}\right] \tag{18}$$

where ρ is the stage correlation coefficient; ΔD_{st} is the difference in excavation depth between the two stages. While Wu et al. (2014) proposed a constant value of θ_{st}, this will be refined under the current framework. Based on multivariate normal theory, the posterior distribution of $\ln \boldsymbol{\varepsilon}^*$ is multivariate normal. The mean and covariance of $\boldsymbol{\varepsilon}^*$ in log-space and original space can be evaluated using ρ:

$$\mathrm{E}(\ln \boldsymbol{\varepsilon}^* | \ln \boldsymbol{\varepsilon}) = (1-\rho)\boldsymbol{\mu}_{\ln \varepsilon} + \rho \ln \boldsymbol{\varepsilon} \tag{19a}$$

$$\mathrm{Cov}(\ln \boldsymbol{\varepsilon}^* | \ln \boldsymbol{\varepsilon}) = (1-\rho^2)\mathbf{C}_{\ln \varepsilon} \tag{19b}$$

$$\mathrm{E}(\boldsymbol{\varepsilon}^* | \boldsymbol{\varepsilon}) = \exp[\mathrm{E}(\ln \boldsymbol{\varepsilon}^* | \ln \boldsymbol{\varepsilon}) + 0.5\mathrm{Var}(\ln \boldsymbol{\varepsilon}^* | \ln \boldsymbol{\varepsilon})] \tag{19c}$$

$$\mathrm{Var}(\boldsymbol{\varepsilon}^* | \boldsymbol{\varepsilon}) = \mathrm{E}(\boldsymbol{\varepsilon}^* | \boldsymbol{\varepsilon})^2 \{\exp[\mathrm{Var}(\ln \boldsymbol{\varepsilon}^* | \ln \boldsymbol{\varepsilon})] - 1\} \tag{19d}$$

Based on similar derivation as in equations (16) and (17), the best estimates and prediction intervals of wall deflections considering stage correlation of bias become:

$$\mathrm{E}(\boldsymbol{y}^*|\boldsymbol{\varepsilon},\boldsymbol{y}) = \mathrm{E}(\boldsymbol{\varepsilon}^*|\boldsymbol{\varepsilon})\mathrm{E}(\boldsymbol{g}^*|\boldsymbol{y}) \tag{20a}$$

$$\mathrm{SD}(\boldsymbol{y}^*|\boldsymbol{\varepsilon},\boldsymbol{y}) = \sqrt{\mathrm{Var}(\boldsymbol{\varepsilon}^*|\boldsymbol{\varepsilon})\mathrm{Var}(\boldsymbol{g}^*|\boldsymbol{y}) + \mathrm{Var}(\boldsymbol{\varepsilon}^*|\boldsymbol{\varepsilon})\mathrm{E}(\boldsymbol{g}^*|\boldsymbol{y})^2 + \mathrm{Var}(\boldsymbol{g}^*|\boldsymbol{y})\mathrm{E}(\boldsymbol{\varepsilon}^*|\boldsymbol{\varepsilon})^2} \tag{20b}$$

The key parameter in determining the stage correlation effects is θ_{st}. This value may be affected by site-specific conditions such as the spatial variability of soil properties or existence of different soil layers, as will be shown in the later examples. The determination of θ_{st} requires a 'back-calibration' procedure, and the details will be illustrated through the following cases.

Illustration by hypothetical scenario

Various components of the proposed approach will be illustrated through two examples of deep excavations, with the first being a hypothetical case. The main advantage of a hypothetical scenario is that all modeling conditions, including soil stress-strain response and spatial distribution of material properties, are assigned and known, so that the capabilities and potential limitations of the proposed updating procedures will not be masked by additional unknowns or assumptions in a real project setting. A three-dimensional (3D) finite difference model of multi-stage excavation in spatially variable soil is first created, using the software *FLAC3D*, as a benchmark model (Fig. 1a). The deflections obtained at two separate locations of the retaining wall in this benchmark model are considered to be 'virtual inclinometer measurements' ($\boldsymbol{y}$) (Fig. 1b). The Bayesian updating analyses are then performed using two-dimensional (2D) finite difference models by *FLAC*, with the 2D simulation results corresponding to $\boldsymbol{g}$ in the proposed framework. Therefore, model bias arises from differences in 2D and 3D

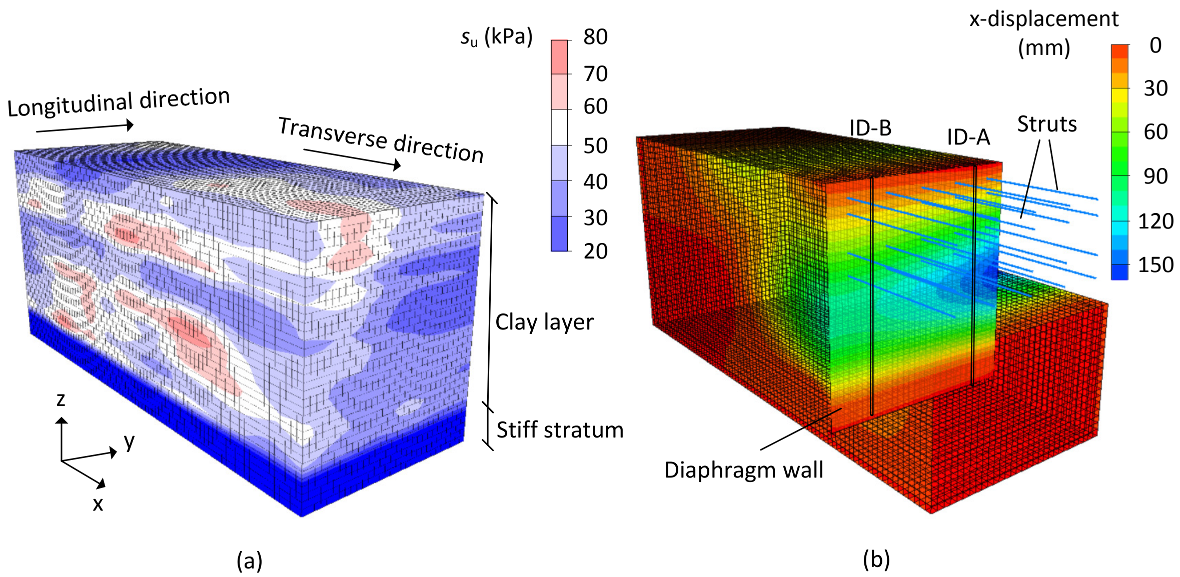

Figure 1: Three-dimensional benchmark model: (a) Spatial distribution of s_{u} profile before excavation; (b) Horizontal displacement after excavation

simulations, and also from the representation of soil variability in these different models. This is intended to imitate the typical scenario encountered by practitioners, where two-dimensional numerical models are often utilized to predict the response of retaining structures or conduct back-analyses from inclinometer measurements.

Geometrical settings of hypothetical excavation case

In the 3D benchmark model, the excavation is 16 m deep and 20 m wide in the transverse direction (representing a half-model). The retaining structure consists of reinforced concrete diaphragm wall, which is 0.9 m thick with a total wall height of 33 m and Young's modulus of 18 GPa. Steel struts are installed at 4 different levels as the excavation progresses (Table 1), at a lateral spacing of 6 m along the longitudinal direction. The struts have cross-sectional area of 0.02 m^2, Young's modulus of 200 GPa and second moment of area of 1.4×10^{-3} m^4. Both the wall and struts are modeled as

Table 1: Construction sequence for hypothetical excavation case

Stage	Depth of strut installation (m)	Excavation depth (m)
1	Nil	3
2	2	5
3	4	10
4	9	13
5	12	16

linear-elastic materials.

The subsurface profile consists of 30 m of 'clayey' material overlying a stiff stratum. The clayey soil has a unit weight of 19 kN/m^3, and its behaviour is modeled by total stress analysis. The undrained shear strength (s_{u}) of the clay is modeled as a lognormal random field, with mean value of 45 kPa and coefficient of variation of 0.4. The horizontal autocorrelation distance ($\theta_x = \theta_y$) is 30 m while the vertical autocorrelation distance (θ_z) is 5 m. The stress-strain response is assumed to be linear-elastic perfectly-plastic in this hypothetical case, and the undrained Young's modulus (E_{u}) is perfectly correlated with the undrained shear strength, with $E_{\mathrm{u}} = 1000s_{\mathrm{u}}$. The Poisson's ratio is assigned to be 0.49 for total stress analysis, and the adhesion factor between the wall and the soil is taken as 0.9. The bottom 3 m of the diaphragm wall is socketed into the stiff stratum, which is assumed to be linear-elastic with Young's modulus of 200 MPa and Poisson's ratio of 0.2.

It is not necessary to generate multiple 3D realizations for this hypothetical scenario, since one 3D model is sufficient to serve as the benchmark. Based on the autocorrelation distances mentioned earlier, the spatial profile shown in Fig. 1a is generated in *FLAC3D*. The mesh size is 1 m$\times$1 m$\times$1 m in the model, with the lateral boundary set at 60 m behind the retaining wall. Roller boundaries are assigned to the four lateral boundaries, while the bottom of the model (35 m below surface) is fixed. The two 'virtual inclinometer' locations are denoted as ID-A and ID-B, where the corresponding deflections will be treated as ‘measurements’ for Bayesian analyses of 2D models. As shown in Fig. 1b, the wall distortion in the longitudinal direction is significant, due to spatial variability of soil properties in that direction.

Two separate 2D *FLAC* models are constructed for the Bayesian updating analyses, at the cross-sections corresponding to inclinometers ID-A and ID-B. The same parameters that characterize random fields of s_u and E_u are adopted in the 2D models, but they involve different spatial variation patterns, due to the different values of $\mathbf{H}^*$ components at the two locations. Based on the soil spatial correlation structure and spectral decomposition of the $\mathbf{R}$ matrix (equation (5)), 39 ξ components are required to capture 95% of the total variance of the random field. 500 realizations of the random field are then simulated using LHSD approach which, as mentioned earlier, is a stratified sampling scheme that preserves the autocorrelation structure of the soil profile (Packham and Schmidt 2010; Lo and Leung 2017). The excavation sequence with the 500 $\boldsymbol{z}$ subsurface profiles are then analyzed by *FLAC*, to obtain 500 deflection estimates for each stage, at each of the two cross-sections. Since deflection ‘measurements’ from the 3D model are separated by 1 m intervals, there are a total of 68 ($n = 68$) deflection values considering the two inclinometers. Therefore, 68 PCE are constructed for each construction stage, with the coefficients obtained through the sparse PCE approach (Blatman and Sudret 2010). Among these measurement points, only those between the depths of 6 to 26 m are used for subsequent Bayesian updating. This is because at the top and bottom of the wall, the deflection values are close to zero, in which case the multiplicative model bias may become unreasonably large, even though the difference in magnitudes between the predicted and measured response is very small. For the selected measurement depths from 6 to 26 m, the cross-validated regression coefficient Q^2 of all the PCE are above 0.93.

Bayesian updating analyses for hypothetical case

While the total variance of the random field may be represented by 39 ξ components, it is beneficial to further reduce the number of components in the Bayesian updating process, since the MCMC algorithm may fail to converge when the number of dimensions is too high. The contributions of individual ξ components are assessed by the Sobol' index, calculated by equation (6), and are summed up across the selected wall points for construction stages 2 to 5. For example, Fig. 2 shows the percentage contribution by the first ten ξ components, where the pattern of Sobol' index variations is similar for all construction stages, with the wall response dominated by the first ξ component. The remaining components are not shown in Fig. 2, but their contributions are generally insignificant, except components 21, 22 and 29, each of which contributing to 1-5% of the response variance. In general, the index does not decrease monotonically, which illustrates that a small-scale spatial variability can still have noticeable effect to the wall deflection response. Based on the Sobol' index analysis, the 9 most influential components (ξ_i) are considered for the updating process, which include components $i = 1$, 4, 2, 21, 6, 3, 7, 29 and 22. Together, these contribute to 86.4%, 92.2%, 94.8% and 95.7% of the deflection response variances at Stages 2, 3, 4 and 5. Subsequently, the number of ξ components to be updated by the Bayesian procedure reduces from 39 to 9, which enhances the robustness of the MCMC algorithm.

As discussed earlier, each measurement location k is associated with a model bias factor ε_k. The $\boldsymbol{\varepsilon}$ vector is assumed to be stationary, and its mean value (μ_ε), standard deviation (σ_ε), and spatial correlation parameters (θ_{spv}, θ_{sph}) will each involve a prior distribution (defined by the mean: $m_{\mu\varepsilon}, m_{\sigma\varepsilon}, m_{\theta spv}, m_{\theta\mathrm{sph}}$ and standard deviation: $s_{\mu\varepsilon}, s_{\sigma\varepsilon}, s_{\theta\mathrm{spv}}, s_{\theta\mathrm{sph}}$), to be updated through the Bayesian procedure using the measurement data (equation (13)). The prior distributions of these model bias factors

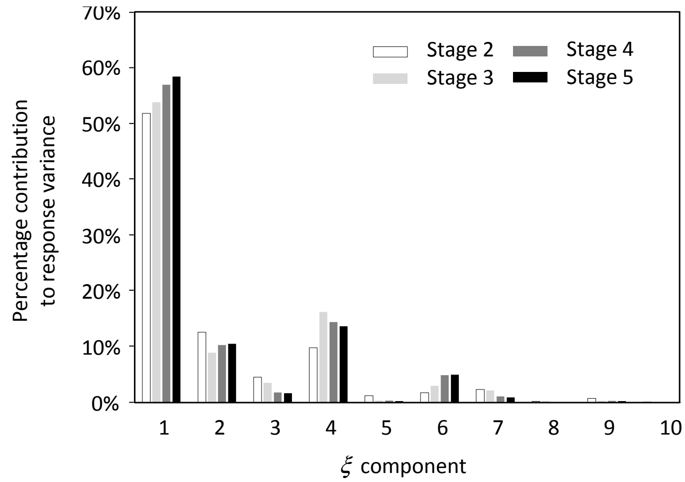

Figure 2: Sensitivity of the first 10 ξ components evaluated by Sobol' index

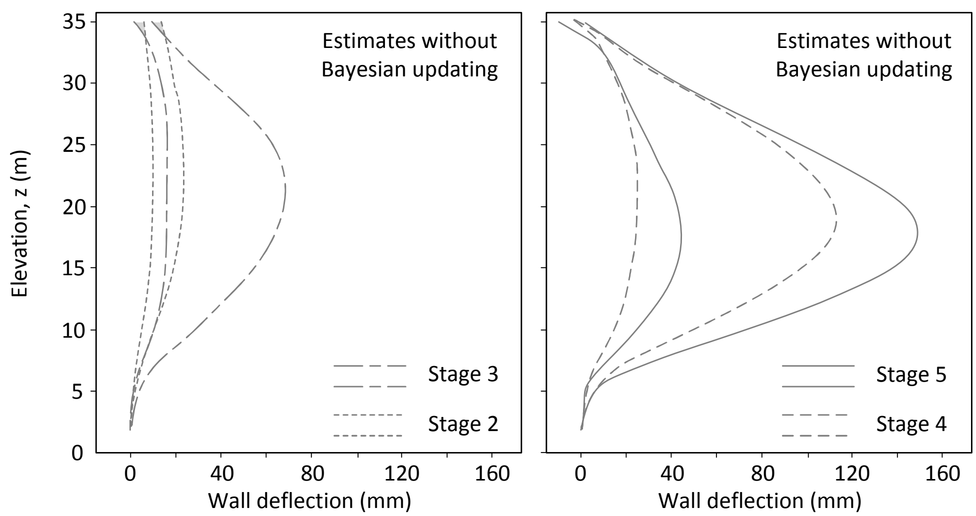

Figure 3: Prior estimates of prediction intervals for hypothetical case

parameters are listed in Table 2, with $m_{\mu\varepsilon} = 1; m_{\sigma\varepsilon} = 0.3$ and $m_{\theta\mathrm{spv}} = 0.7$, similar to the recommendations by Qi and Zhou (2017). There has been limited discussions in the literature on the value of θ_{sph}. In this analysis, it is assumed that the prior mean $m_{\theta\mathrm{sph}} = 1.87$, which corresponds to the horizontal autocorrelation distance of the s_{u} random field. The standard deviations of the prior distributions for these parameters are also shown in Table 2. Based on the prior distributions of the 9 ξ components (N(0,1))

Table 2: Spatial correlation of model bias factor: hypothetical case

Model bias parameters	Prior mean	Prior SD	Stage 2 mean	Stage 2 SD	Stage 3 mean	Stage 3 SD	Stage 4 mean	Stage 4 SD
μ_ε	1	0.05	1.02	0.039	1.02	0.035	1	0.032
σ_ε	0.3	0.15	0.1	0.015	0.14	0.01	0.16	0.009
θ_{spv}	0.7	0.3	0.6	0.06	0.58	0.061	0.67	0.055
θ_{sph}	1.87	0.5	1.41	0.355	1.05	0.304	1.23	0.25

and 4 model bias factors, the prior prediction intervals for all stages (without subsequent updating) can be evaluated, as shown in Fig. 3. Due to the substantial model and soil spatial uncertainty, the resulting prediction intervals are fairly wide, especially for the later stages of construction, and may not provide much useful information for practical purposes. In addition, this prior prediction does not differentiate between the response in the two cross-sections arising from the soil variability along the longitudinal direction.

Table 3: Bayesian updating of ξ components: hypothetical case

Components of soil variability	Prior mean	Prior SD	Stage 2 mean	Stage 2 SD	Stage 3 mean	Stage 3 SD	Stage 4 mean	Stage 4 SD
ξ_1	0	1	-0.59	0.17	-0.95	0.1	-1.01	0.08
ξ_2	0	1	-0.07	0.15	-0.22	0.08	-0.21	0.06
ξ_3	0	1	-0.41	0.17	-0.61	0.11	-0.57	0.08
ξ_4	0	1	1.03	0.2	0.57	0.16	0.15	0.12
ξ_6	0	1	-0.22	0.11	-0.21	0.07	-0.15	0.06
ξ_7	0	1	-0.14	0.17	-0.06	0.09	-0.11	0.06
ξ_{21}	0	1	0.67	0.26	0.49	0.15	0.67	0.12
ξ_{22}	0	1	0.13	0.19	-0.08	0.1	-0.11	0.08
ξ_{29}	0	1	-0.23	0.22	0.11	0.12	0.03	0.1

The Bayesian updating is performed through the AM algorithm for MCMC, described in equation (14). The Markov chain has a total chain length of 40000, with an initial burn-in period of 5000. The adaptation starts at chain length (t_0) of 10000, before which the acceptance rate of the Markov chain ranges from 5-10%. After the commencement of adaptation ($t > t_0$), the acceptance rate gradually increases to about 50%.

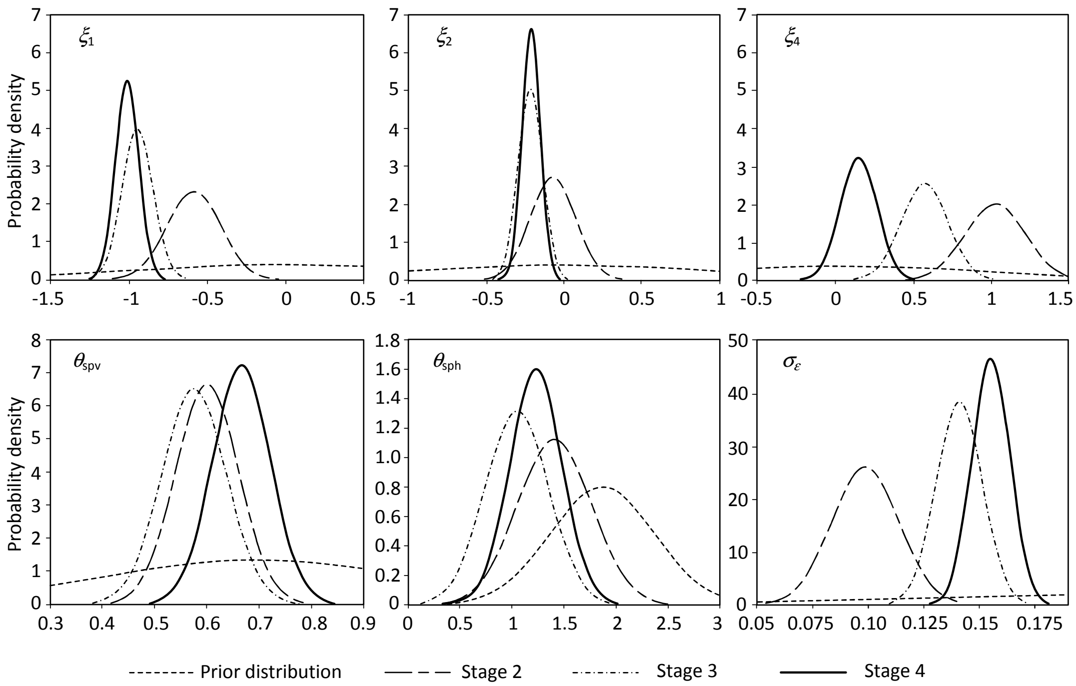

Figure 4: Prior and posterior distributions for three ξ components and three model bias parameters

In the Bayesian process, the posterior distribution obtained at a certain construction stage is used as the prior for the next stage. Tables 2 and 3 show the posterior distribution of the ξ components and model bias parameters after each updating stage, while Fig. 4 also shows the distributions for some of the parameters. The results show that the standard deviations of both ξ components and $\boldsymbol{\varepsilon}$ parameters decrease monotonically through repeated updating and refining of parameters, with the most significant reduction occurring at Stage 2. The normalized vertical and horizontal autocorrelation distances of $\boldsymbol{\varepsilon}$ are about 0.67 and 1.23, which correspond to 10.7 m and 19.7 m by multiplying with H, showing that the model bias can be spatially anisotropic. Meanwhile, based on the sequentially updated $\boldsymbol{\varepsilon}$ and $\boldsymbol{\xi}$ parameters, the prediction intervals are evaluated by equation (17) and shown in Fig. 5. As mentioned earlier, the prediction intervals for a certain stage are based on the updated parameters obtained at the immediate previous stage. For example, the prediction intervals for stage 3 are evaluated using the posterior distribution of parameters obtained at the end of stage 2. In general, the prediction intervals (mean estimate plus/minus one standard deviation) from the 2D models can envelope the actual deflection from 3D benchmark simulation at a reasonable width. The approach also allows the longitudinal distortion of the retaining wall to be encapsulated, with different response predicted for the two cross-sections ID-A and ID-B.

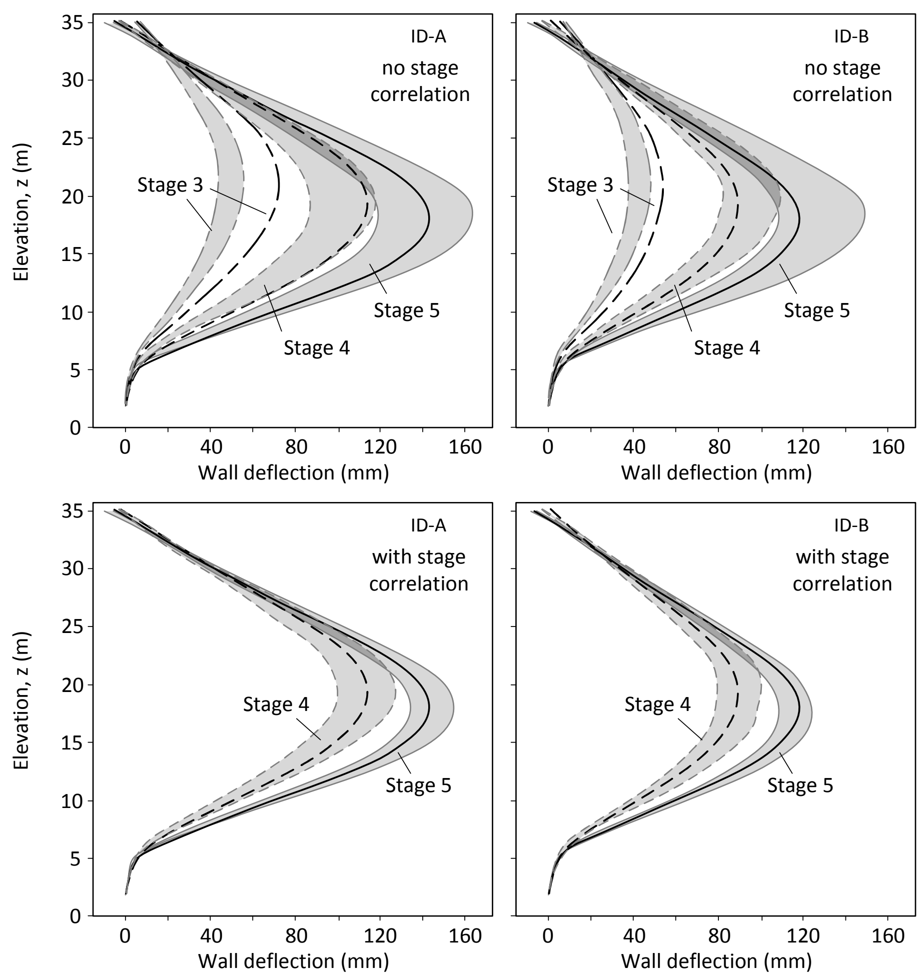

Figure 5: Measured wall deflection (black) and prediction range (grey) for hypothetical case

The stage correlation of model bias is determined through a 'back-calibration procedure. For example, at the end of stage 4, the deflections of stages 3 and 4 can be back analyzed using the mean of updated parameters in stage 4. If the realized model bias of the stage 4 is denoted as $\ln \boldsymbol{\varepsilon}_4$, and that of stage 3 as $\ln \boldsymbol{\varepsilon}_3$, the correlations between $\ln \boldsymbol{\varepsilon}_3$ and $\ln \boldsymbol{\varepsilon}_4$ can be assessed by fitting a 1:1 line (Fig. 6), and the goodness of fit is evaluated by R^2:

$$R^2 = 1 - \frac{\sum_n (\ln \boldsymbol{\varepsilon}_4 - \ln \boldsymbol{\varepsilon}_3)^2}{n\sigma^2_{\ln \varepsilon}} \tag{21}$$

If $R^2 > 0$, the stage correlation coefficient is estimated as $\rho = \sqrt{R^2}$, and the stage autocorrelation distance is evaluated by $\theta_{\mathrm{st}} = -\Delta D_{\mathrm{st}} / \ln \rho$ (equation (18)).

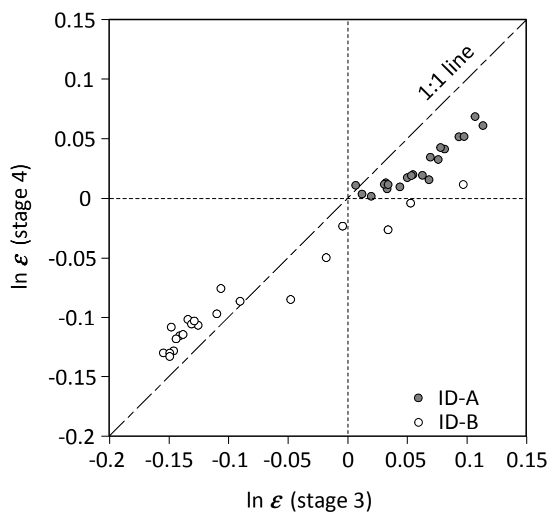

Figure 6: Example of correlation between model bias in different stages of hypothetical case

For this hypothetical case, at the end of stage 4, the ρ values between stages 2-3, stages 2-4 and stages 3-4 are 0.86, 0.92 and 0.97, which corresponds to θ_{st} of 33.2 m, 91.8 m and 96.9 m, respectively. The smallest value of 33.2 m is adopted, which may be considered to be conservative, as the width of prediction interval increases with reducing ρ (equation (19)). Based on θ_{st} computed at the end of stage 3 (not shown) and stage 4, the refined prediction intervals of stage 4 and stage 5 are computed by equation (20) and are shown in Fig. 5. Compared to the estimates without stage correlation, the refined intervals are narrower, and the actual deflection lies in the center of the refined intervals.

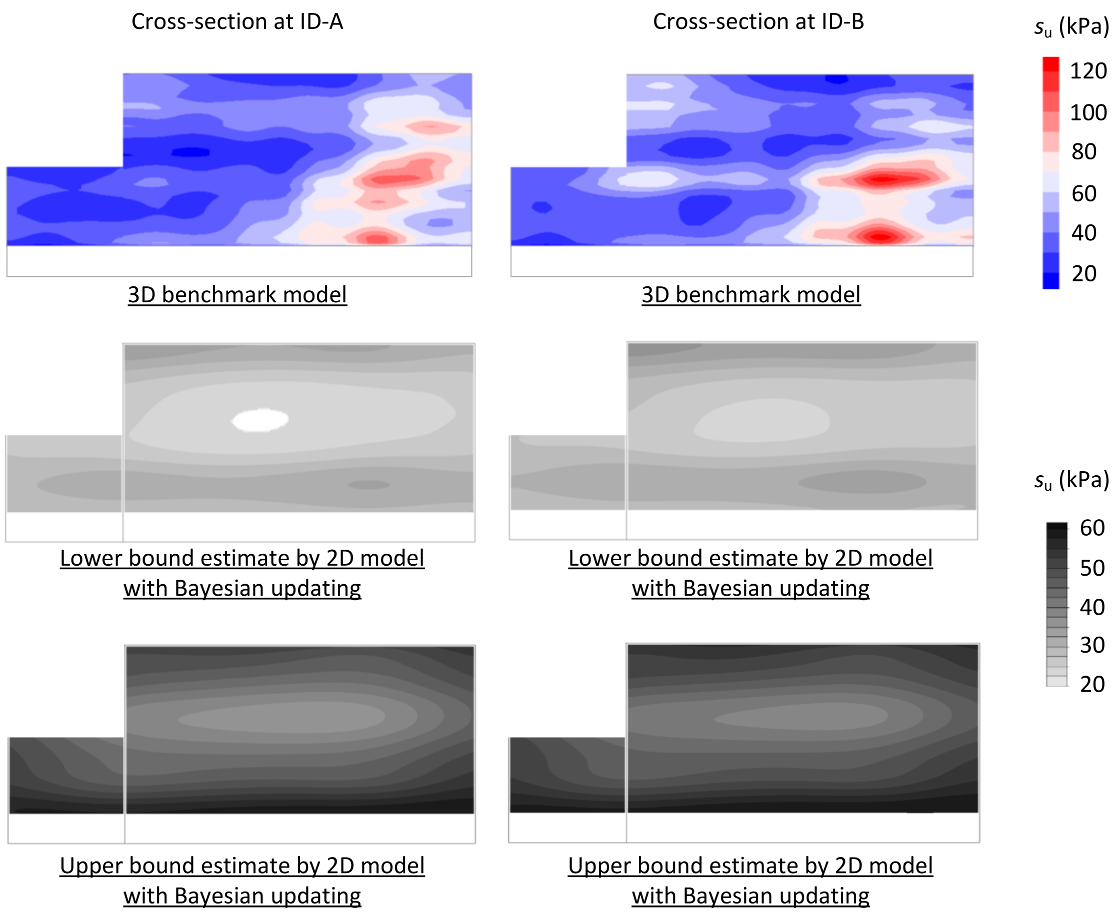

Figure 7: Comparisons between s_u profiles in 3D benchmark model and posterior estimates by 2D models

Fig. 7 shows the posterior estimates (mean plus and minus standard deviation) of s_u profiles at the ID-A and ID-B locations, updated based on equation (16) after stage 4. Considering the intrinsic differences between 2D and 3D simulations, the variation patterns of the benchmark model are reasonably well captured by the 2D models, with higher shear strength close to the wall, and weaker soils towards the center of the model. Also, the posterior s_u estimates are generally higher at the ID-B model, which are reflected in the smaller wall deflections. Although the very strong soils ($s_u > 80$ kPa) near the boundaries of the 3D benchmark model cannot be captured by the updating process, they are deemed to be too far behind the retaining wall with insignificant influence to the wall deflections.

Application to excavation project in Hong Kong

Description of site conditions

The second case involves the Bayesian analyses of a deep excavation project during construction of the West Rail Line of the Mass Transit Railway (MTR) in Hong Kong. The project background, details of site conditions and data of displacement measurements have been reported by Pickles et al. (2006), with the project layout shown in Fig. 8. The project site is located in the Tsuen Wan area in Hong Kong, where a 400-m long underground station and 600 m of cut-and-cover tunnels, separated into the Northern Approach Tunnel (NAT) and Southern Approach Tunnel (SAT), were constructed in the early 2000s. Extensive geotechnical investigation and site instrumentation were implemented prior to and during construction of the station and tunnels. In this study, a section of the deep excavation at NAT is investigated, where the inclinometer measurements of diaphragm wall deflections are used to update the subsurface soil variability and model bias, and to sequentially refine the predictions for later stages.

The construction site is located at an area that had undergone multiple phases of previous reclamation. At the NAT section, the reclamation was completed more than 10 years before construction of the tunnel. The subsurface profile consists of 12.5 m of fill, overlying a 2.5-m layer of marine deposits. Below the marine deposit is a thin layer (around 0.5 m thick) of alluvium, followed by completely decomposed granite (CDG) which is 9 m thick. Both the marine deposit and alluvium layers composed of silty and clayey sand materials, with variable amounts of gravel. The rock (granite) stratum

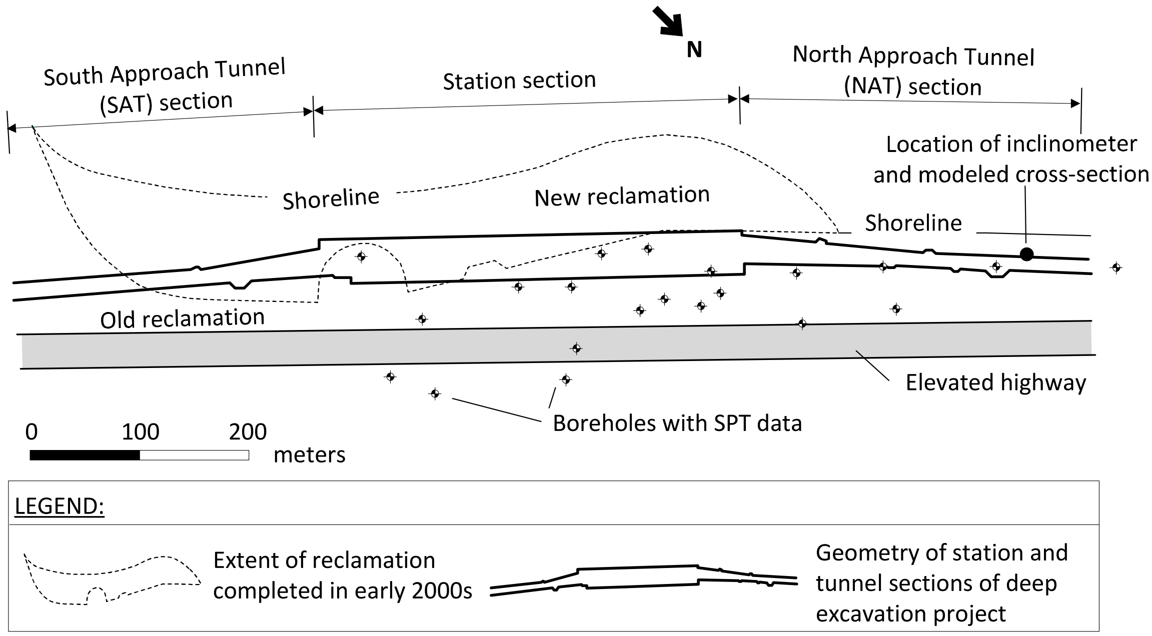

Figure 8: Layout of the Tsuen Wan excavation project and locations of boreholes (adapted from Pickles et al. (2006))

is approximately 24.5 m below the ground surface, or at reduced level of -19.8 mPD (Principal Datum of Hong Kong is 1.230 m below mean sea level). The water table was at +2 mPD, which was about 2.7 m below the ground surface.

The lateral support system at the NAT excavation consisted of reinforced concrete diaphragm wall which was 0.8 m thick, with a total wall height of 30.5 m, and the bottom 6 m of the wall was embedded in rock. The total excavation depth was 19.5 m, with four levels of temporary steel struts. The steel struts were double UB $610 \times 324 \times 174$ sections modeled as linear-elastic material, with Young's modulus of 200 GPa, cross-sectional area of 0.0456 m^2 and second moment of area of 1.53×10^{-3} m^4. The lateral spacing of the struts was 7 m. The diaphragm wall was constructed with tremie concrete. Considering the concreting process which was performed under water, the concrete is assumed to have a Young's modulus of 18 GPa in the subsequent analyses. Also, in the following simulations of the excavation process (Table 4), the groundwater level is

Table 4: Construction sequence for Tsuen Wan excavation case

Stage	Depth of strut installation (m)	Excavation depth (m)	Depth of water level inside cofferdam (m)
1	Nil	1.5	2.5
2	1	5.5	6.5
3	5	9.5	10.5
4	9	12.5	13.5
5	Nil	15	16
6	14.5	19.5	20.5

lowered to 1 m below the excavated level inside the cofferdam. Behind the diaphragm wall, the groundwater level is maintained at a constant level of +2 mPD. Monitoring data of the diaphragm wall deflections is available through inclinometer readings as the construction progresses. It should be noted that at stage 1 where excavation depth was around 1.5 m, the 'measured' maximum deflection was already 25 mm according to the original records. This unexpectedly large value was likely due to the installation of the inclinometer casing or other processes that had occured before the excavation. The deflection values at this stage is therefore taken as a constant baseline value, and deducted from the measurements at subsequent stages.

Modeling of soil variability

Since the marine deposit and alluvium layers are relatively thin, with combined thickness of only 3 m, their properties are modeled as constants. The number of soil samples retrieved for laboratory testing was very limited. In fact, for the fill and CDG materials which compose of silty and sandy soils, laboratory test results for shear strength and stiffness may be affected by disturbance during retrieval and handling of the specimens. Therefore, in this study, the prior distributions for spatial variability of soil strength and stiffness are derived through results of in situ standard penetration tests (SPT). The records of 21 boreholes around the station and NAT areas (Fig. 8) are utilized, which provide 94 data points of SPT blow counts (N values) in the fill layer, and 40 data points in the CDG layer. Based on the field data, Fig. 9 shows the spatial correlation features of fill and CDG layers in both horizontal and vertical directions, established using the Restricted Maximum Likelihood (REML) method (e.g., Cressie and Lahiri 1996; Lark and Cullis 2004; Minasny and McBratney 2005; Liu et al. 2017), which allow the derivation of autocorrelation distances (equation (2)). These are also compared with discrete estimates by the method of moments (MoM) for reference. Although the two methods agree less well in some cases, Liu et al. (2017) showed that REML is statistically more robust with a small dataset. Therefore, the θ_x, θ_y and θ_z values are adopted based on REML estimates. As mentioned earlier, it is also possible to adopt other functional forms of $\mathbf{R}$, such as the single exponential function. In that case, the corresponding θ values obtained by REML will be larger than those in Table 5, in order to match the spatial variability features displayed by the site data. This will also lead to similar results in the updating analyses. Meanwhile, it should be noted that the estimation of spatial correlation parameters using sparse measurements may be affected by statistical uncertainty, an issue which has been discussed in length by Ching et al. (2016). While this study advocates enhanced utilization of available soil data with the spatial information, such potential limitation should be noted especially when the amount of site-specific information is very limited.

To convert the SPT-N values into soil stiffness distributions, the maximum shear modulus (G_0) is estimated by:

$$G_0 = \rho_s V_s^2 = \rho_s \left[27(N_{60}\,\sigma'_v)^{0.23}\right]^2 \tag{22}$$

where ρ_s is the soil density and σ'_v represents the vertical effective stress at the sampling depth; the relationship between shear wave velocity (V_s) and N_{60} was proposed by Wair et al. (2012) for sandy materials. SPT are conducted by mechanized hammers with energy efficiency of around 80% in the local practice. This is considered in the conversion from N into N_{60}.

A two-dimensional *FLAC* model is used to simulate a cross-section in the NAT section of the project. In theory, it is possible to simulate multiple cross-sections as in the hypothetical case. This is, however, not performed because the next inclinometer is located more than 50 m away from this cross-section, and the spatial correlations between the two locations, in both the soil properties and model bias, are deemed to be insignificant. Table 5 summarizes the soil properties adopted in the numerical model, with the mean values similar to those adopted in deterministic analyses by Pickles et al. (2006). In this study, a shear hardening soil constitutive model is adopted ('Chsoil' model) in *FLAC*, which features a hyperbolic function representing the shear stress-strain relationship:

$$G_{\mathrm{p}} = G_0 \left[1 - \frac{\sin\phi_{\mathrm{m}}}{\sin\phi_{\mathrm{p}}} R_{\mathrm{f}}\right]^2 \tag{23}$$

where ϕ_{p} is the peak friction angle, ϕ_{m} is the mobilized friction angle, and R_{f} is the failure ratio taken as 0.9. G_0 is the initial (elastic) shear modulus, which is also the unloading-reloading shear modulus; G_{p} represents the plastic shear modulus according to the mobilized ϕ_{m}.

Table 5: Soil properties adopted in Tsuen Wan excavation case

	γ (kN/m^3)	Mean G_{ref} (MPa)	CV: G_{ref}	Mean ϕ_{p}	CV: ϕ_{p}	θ_x, θ_y (m)	θ_z (m)
Fill	19	44.2	0.15	34°	0.15	80	1
Marine deposit	19	67	–	34°	–	–	–
Alluvium	19	67	–	34°	–	–	–
CDG	19.5	90	0.25	37°	0.15	222	11

*γ: unit weight; CV: coefficient of variation

During the excavation process, the stress field in the soil will be altered and its shear

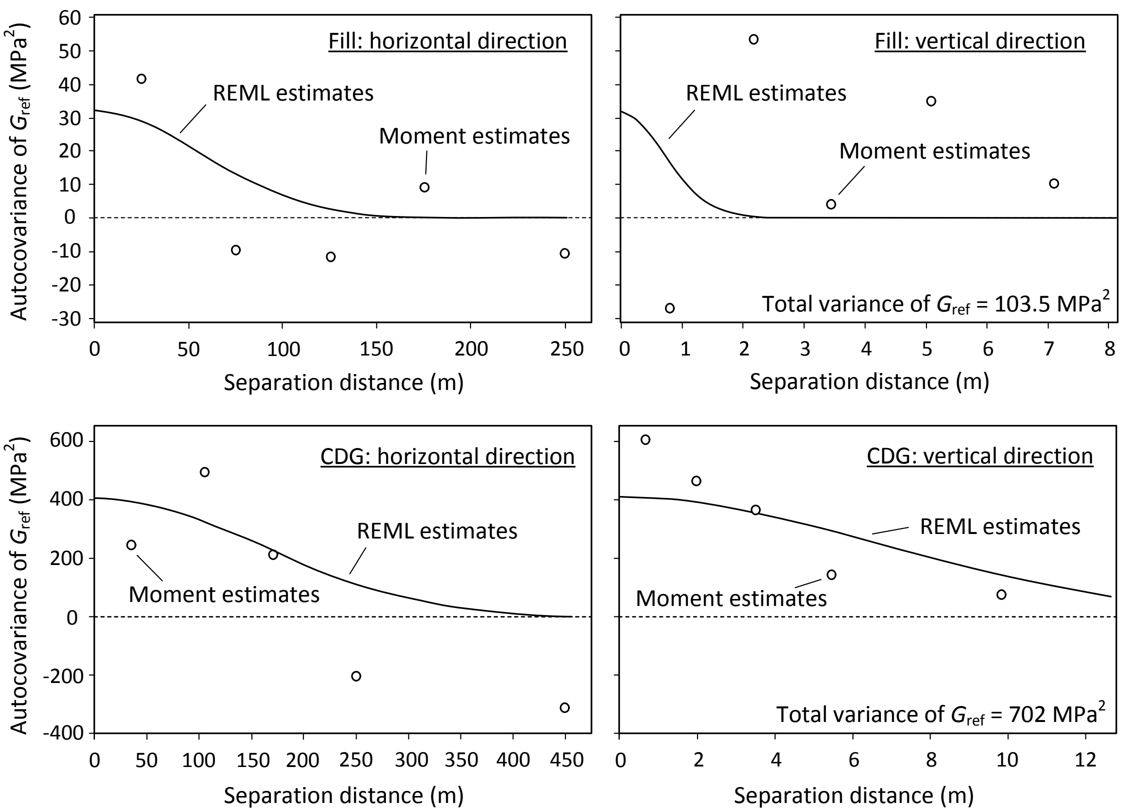

Figure 9: Spatial correlation of G_{ref} for fill and CDG layers, estimated by restricted maximum likelihood method and the method of moments

stiffness will be affected correspondingly. Therefore, instead of a random field of G_0, this study utilizes random field of the 'reference' modulus G_{ref}, which is related to G_0 by:

$$G_0 = G_{\mathrm{ref}} \left(\frac{p'}{p_{\mathrm{a}}} \right)^m \tag{24}$$

where p' is the mean effective stress in the soil, p_{a} is the atmospheric pressure (100 kPa) and m is a modulus exponent taken as 0.5 in this study. Equation (24) is conceptually similar to the stress-dependent model proposed by Duncan and Chang (1970). The mean values of ϕ_{p} are taken to be 34° and 37° for fill and CDG (Pickles et al. 2006), while the coefficient of variation of ϕ_{p} for both layers are assumed to be 0.15, which is consistent with the range reported in Phoon and Kulhawy (1999). Meanwhile, ϕ_{p}

is assumed to be perfectly correlated with G_{ref}. While soil strength and stiffness are expected to be positively correlated, the precise degree of cross-correlation is rarely reported. This study assumes the cross-correlation coefficient to be unity, and it is possible to incorporate other values of the coefficient, although this would lead to a more sophisticated mathematical formulation. In addition, the peak dilatancy angle is assumed to be equal to $\phi_{\mathrm{p}} - 30°$ (with minimum value of 0), which is an approximation also adopted by Sert et al. (2016). The soil-wall interface is assumed to have a constant friction angle of 24.5°, which roughly corresponds to interface reduction factor of 0.65 and is in line with the recommendations of local design guidelines.

Without extensive and high-quality sampling and laboratory testing for soils at the site, the adopted equations (22) to (24) will inevitably introduce transformation uncertainty. In this case, this component of geotechnical uncertainty is treated together with model uncertainty, through sequential updating of the model bias factors in the Bayesian process. In cases where large amounts of site-specific triaxial test data is available, the corresponding soil stress-strain relationships can be established with better confidence, and the associated transformation uncertainty can be substantially reduced.

Bayesian updating analyses for excavation case study

Based on the random field characteristics in Fig. 9 and Table 5, 500 realizations are generated by the LHSD method. The realizations are simulated by *FLAC* to obtain 500 deflection profiles. The number of measurement points is 61, as the interval of inclinometer readings, and the mesh size for the retaining wall in the numerical model are 0.5 m. Therefore, 61 PCE are fitted for each construction stage, using the SPCE approach. Similar to the hypothetical case, only the middle section of the inclinometer (elevation of 0.2 mPD to -14.8mPD) is used for updating, as the multiplicative model bias may become unreasonably large at the end regions. Within the selected section, the

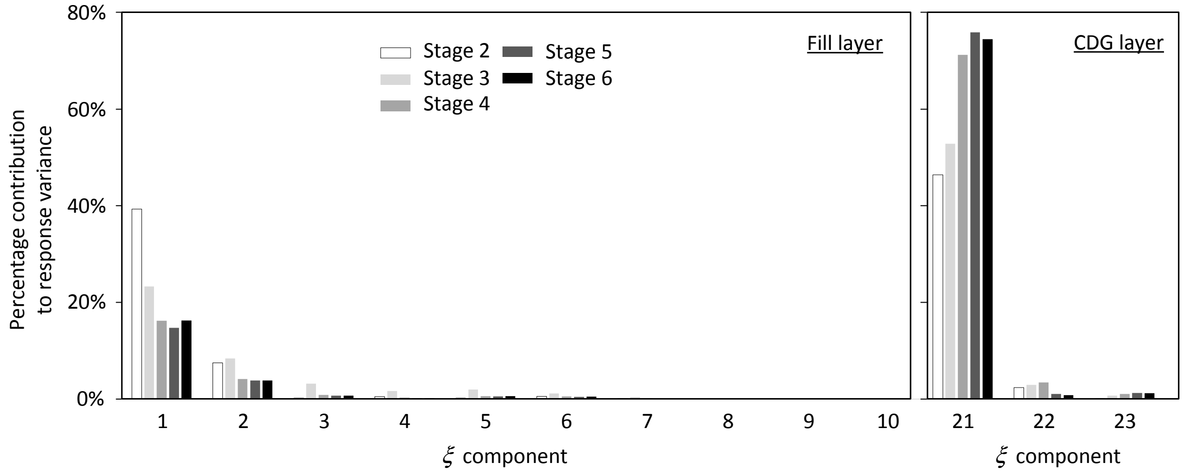

Figure 10: Sensitivity of the first 10 ξ components in fill layer, and 3 ξ components in CDG layer

cross-validation coefficients Q^2 of the fitted PCE all exceed 0.93. 23 ξ components are required to capture 95% of the random field variance, with components 1-20 representing fill, and components 21-23 representing CDG. Before the Bayesian updating process, Sobol' index analysis is conducted to select the influential ξ components for updating, and the results are shown in Fig. 10. At the early stage of the excavation, when the excavation depth is shallow, fill and CDG have similar influences towards the wall response. As the excavation depth becomes deeper, CDG becomes more influential. Also, the Sobol' index does not decrease monotonically with ξ components. As shown in Fig. 10, the six most influential components are numbers 21, 1, 2, 22, 3, 23. Together, these account for the majority of variance in wall response, representing 95.8%, 91.3%, 96.9%, 97.5% and 97.3% at stages 2, 3, 4, 5 and 6, respectively.

The prior mean and SD of the model bias parameters are the same as the hypothetical case. The Bayesian updating is performed with the AM algorithm, and the Markov chain has a total chain length of 40000, with an initial burn-in period of 5000. The adaptation starts at chain length of 10000, before which the acceptance rate of the Markov chain ranges about 5-15%. After the adaptation, the acceptance rate gradually rises to about 60%. The posterior distribution obtained at a certain construction stage is used as the prior distribution for the next stage.

Table 6: Spatial correlation of model bias factor: Tsuen Wan case

Model bias	Prior		Stage 2		Stage 3		Stage 4		Stage 5	
parameters	mean	SD	mean	SD	mean	SD	mean	SD	mean	SD
μ_ε	1	0.05	0.99	0.046	1.03	0.044	1.04	0.040	1.04	0.036
σ_ε	0.3	0.15	0.28	0.045	0.21	0.043	0.23	0.025	0.22	0.021
θ_{spv}	0.7	0.3	0.37	0.078	0.23	0.048	0.42	0.06	0.36	0.064

Table 7: Bayesian updating of ξ components: Tsuen Wan case

Components of	Prior		Stage 2		Stage 3		Stage 4		Stage 5	
soil variability	mean	SD	mean	SD	mean	SD	mean	SD	mean	SD
ξ_1	0	1	-0.08	0.87	0.09	0.49	0.25	0.38	-0.13	0.33
ξ_2	0	1	0.01	0.98	0.32	0.79	0.68	0.66	1.02	0.57
ξ_3	0	1	-0.47	0.72	0.02	0.42	-0.33	0.32	-0.1	0.28
ξ_{21}	0	1	-0.02	0.67	1.53	0.39	1.80	0.26	1.51	0.22
ξ_{22}	0	1	0.18	0.94	-0.3	0.57	-0.29	0.45	-0.39	0.38
ξ_{23}	0	1	0.01	0.72	0.19	0.52	0.50	0.44	0.28	0.38

Tables 6 and 7 shows the posterior mean and SD of the ξ components and model bias parameters. In general, the SD keep decreasing through repeated updating, with the effects more notable for soil variability parameters (ξ components), and less significant for the model bias parameters. At the final stage, the normalized vertical autocorrelation distances (θ_{spv}) of $\boldsymbol{\varepsilon}$ is 0.36, which corresponds to approximately 7 m. Based on the updated $\boldsymbol{\xi}$ and model bias, the prediction intervals at each stage can be evaluated, and are shown in Fig. 11. The predictions of stages 4 and 6 show considerable improvement over the prior estimates (with no updating), with the prediction intervals being closer to the actual deflection curves. For stage 5, the improvement is not obvious, which may be due to the excavation into different soil layers at this stage. It is also worth noting that, compared to the prior estimates, the width of prediction intervals only reduces slightly after the Bayesian updating analyses. This is mainly attributable to two reasons: (1) the variance of model bias (σ_ε) is not significantly reduced by the updating process; and (2) the wall deflection estimates $\boldsymbol{g}^*$ is increased by updating, and together with the multiplicative model bias, the prediction interval due to model bias would expand, which counterbalances the reduced soil variability and model uncertainty.

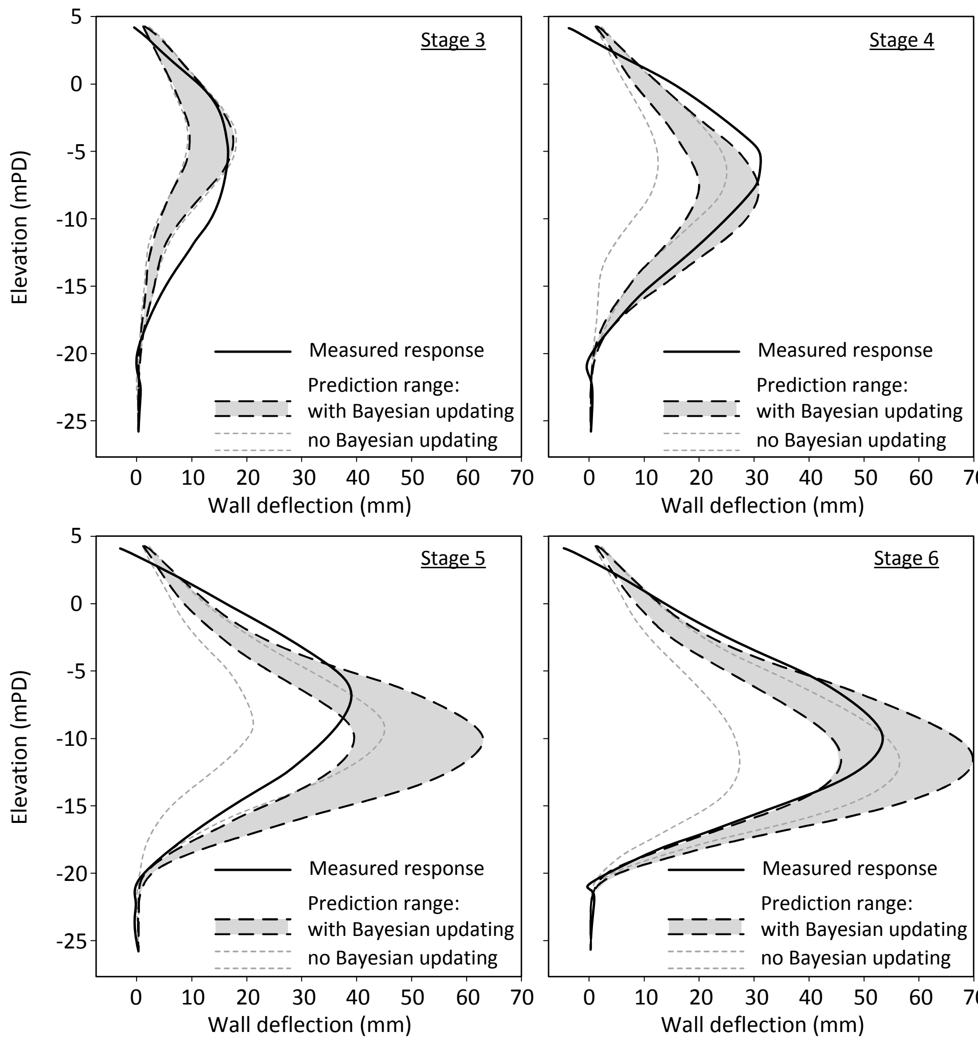

Figure 11: Measured wall deflection and prediction range (mean plus/minus one standard deviation) at Tsuen Wan case

Unlike the hypothetical scenario, the stage correlation in this case is found to be insignificant. For example, Fig. 12 compares the model bias of stages 2 and 5, which

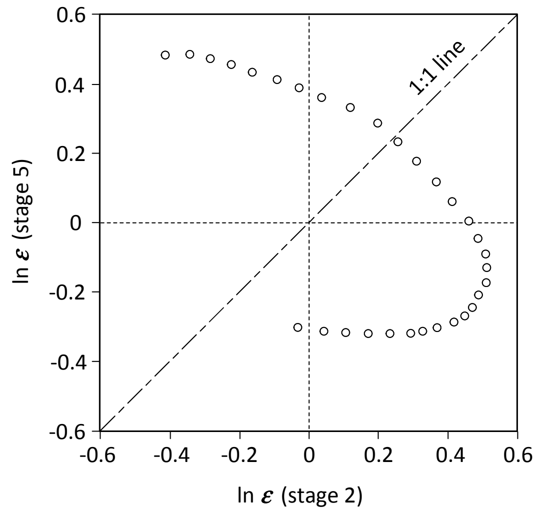

Figure 12: Example of correlation between model bias in different stages of Tsuen Wan case

does not show any clear pattern of correlations. Therefore, further refinements of the prediction intervals are not performed. This may be attributed to the fact that the excavation is performed in four different soil layers, each having different mean values and variation features in the properties, causing the stage correlation effects to be less significant than the hypothetical excavation in a statistically homogeneous material.

Discussions

Fuentes et al. (2018) recently reported the lessons learned from a deep excavation project where the observational method was adopted. The relevant key requirements from Eurocode 7 (British Standards Institute 2004) are also summarized in Spross and Johansson (2017), which include: (1) definition of acceptable limits of the system behavior; (2) assessment on the range of possible behavior, with an acceptable probability that the actual behavior will be within acceptable limits; (3) monitoring plan with frequent measurements so that contingency measures can be implemented if and when necessary; (4) rapid response time for instruments and analyses of monitoring results; and

(5) plans of contingency actions if the monitoring reveals behaviour outside acceptable limits.

With the analytical components presented in this paper, the proposed approach may serve as a quantitative tool under the framework of the observational method. In a braced excavation project, the acceptable wall deflection criteria would be assigned according to site conditions such as proximity to sensitive structures. While probabilistic analyses provide a means to establish the possible system response (e.g., wall deflection), the proposed Bayesian approach allows the probabilistic estimates to be progressively refined and updated through monitoring results such as inclinometer readings. For example, based on inclinometer reading $\boldsymbol{y}$ at a certain stage, the prediction intervals of wall deflection at subsequent stages (i.e., $\boldsymbol{y}^*|\boldsymbol{y}$) can be updated by equation (17). In the preceding hypothetical scenario and case study, the prediction intervals are presented as mean estimate plus/minus one standard deviation, which corresponds to confidence interval of roughly 68%. It is also possible to present the confidence interval of 95%, using mean plus/minus two standard deviations. These intervals provide quantitative indicators on the probability of system behavior exceeding certain limits. It would be a cause for concern if field measurements exceed the prediction intervals, as this implies that some elements of uncertainty may not have been properly accounted for.

The confidence levels should be assessed and interpreted together with the tolerable risk level of the project, which should be agreed upon by all the stakeholders and decision-makers. For example, remedial actions may be initiated if the estimated mean and standard deviations of wall deflections point to a high probability for future response to exceed acceptable limits, as outlined in criteria (1) and (2) above. During the course of construction, it is also essential that these decisions are made considering all available information, to avoid a false sense of security (or false alarm). In the current context, this refers to the consideration of site-specific soil sampling data when establishing the spatial correlation structure, which is then explicitly modeled and progressively refined as inclinometer readings are obtained. The approach involves data-driven procedures that are representative of the specific project conditions. The importance of this refinement process can be recognized by comparing the analyses with and without Bayesian updating, in Figs. 5 and 11.

The observational method requires rapid response time regarding analyses of monitoring data and their implications to the subsequent response. While the proposed approach involves probabilistic analyses with about 500 *FLAC* simulations, which can take days to complete, it is important to note that these random field simulations would be performed during the planning stage, prior to commencement of construction. Once the excavation starts with incoming monitoring data, the updating algorithm only involves evaluations that can be completed quickly (e.g., less than an hour even for the real construction case), so that necessary remedial measures can be implemented without delay. This updating operation is, arguably, not slower than inverse analyses of the data using finite element or finite difference analyses based on deterministic approach.

While this study focuses on incorporating spatial variability of soil properties into the Bayesian framework, it is also possible to include variability in the geological profiles and soil layer thickness. This is, however, not considered in the presented case study, where information on soil strata was obtained from a nearby borehole about 10 m away from the cross-section. Due to the close proximity between this borehole and the inclinometer, the uncertainty on layer thickness is deemed to have insignificant contributions to the modeling results. Moreover, including uncertainty in soil layering will lead to more complications in the formulation, as each numerical realization will entail a different number of elements for each soil layer. The implementation of such modeling scheme may be explored in a future study.

Conclusion

This paper incorporates the Bayesian approach with surrogate modeling technique, to update the principal components that characterize the spatial variability of soil properties using field measurements of system response. The approach also allows the model bias factors, their spatial and stage-dependent correlations to be considered, so that response predictions for the subsequent stages can be continuously refined as the construction progresses.

Two deep excavation cases are presented to illustrate the capabilities of the proposed approach. The hypothetical case shows that using separate 2D analysis models, the approach can capture the distortion phenomenon along the longitudinal direction of the retaining wall, which arises due to spatial variability of the soils in lateral directions. The second illustration involved an excavation case study in Hong Kong, where the updating approach is able to envelope the measured deflection response, considering site-specific data that reveals the variability features in soil properties. The two cases also revealed the merits and limitations of the stage correlation model for bias factor: while stage correlation improves the prediction accuracy when the excavation is conducted within a statistically homogeneous material, it is less effective when the excavation involves multiple soil layers with abruptly changing properties.

In addition, it should be noted that the two presented cases are not 'back-analysis' exercises where the model parameters are calibrated to produce numerical results that match the measurements. Instead, the soil properties are derived using in situ test data, together with well-established strength and stiffness relationships. Predictions for later stages are sequentially updated and refined using wall response measurements obtained as the construction progresses, meanwhile incorporating various sources of uncertainty. The role of this proposed approach within the framework of observational method is elucidated, as the refined estimates and prediction intervals can help support the decision-making process regarding the subsequent excavation stages.

Acknowledgement

The work presented in this paper is financially supported by the Research Grants Council of the Hong Kong Special Administrative Region (Project No. 25201214). In addition, the authors would like to acknowledge the advice by Dr S.W. Lee of Golder Associates, regarding the details of the Tsuen Wan excavation case study. Mr Kerwin Lee also assisted in collecting the data for the Tsuen Wan case, and setting up the numerical models for the *FLAC* analyses.

References

Al-Bittar, T. and Soubra, A.-H. 2014. “Probabilistic analysis of strip footings resting on spatially varying soils and subjected to vertical or inclined loads.” *J. Geotech. Geoenviron. Eng.*, 10.1061/(ASCE)GT.1943-5606.0001046, 04013043.

Anderson, T. W. 1984. *An introduction to multivariate statistical analysis*. John Wiley & Sons, Inc.

Baecher, G. B. and Christian, J. T. 2003. *Reliability and Statistics in Geotechnical Engineering*. Wiley.

Baroth, J. and Malecot, Y. 2010. “Probabilistic analysis of the inverse analysis of an excavation problem.” *Computers and Geotechnics*, 37(3), 391 – 398.

Blatman, G. and Sudret, B. 2010. “An adaptive algorithm to build up sparse polynomial chaos expansions for stochastic finite element analysis.” *Probab. Engrg. Mech.*, 25, 183–197.

British Standards Institute 2004. *Eurocode 7: Geotechnical design - Part 1: General Rules.*

Ching, J., Phoon, K.-K., and Chen, Y.-C. 2010. "Reducing shear strength uncertainties in clays by multivariate correlations." *Canadian Geotechnical Journal*, 47(1), 16–33.

Ching, J., Wu, S.-S., and Phoon, K.-K. 2016. "Statistical characterization of random field parameters using frequentist and bayesian approaches." *Canadian Geotechnical Journal*, 53(2), 285–298.

Cressie, N. and Lahiri, S. N. 1996. "Asymptotics for REML estimation of spatial covariance parameters." *Journal of Statistical Planning and Inference*, 50(3), 327–341.

Duncan, J. M. and Chang, C. Y. 1970. "Nonlinear analysis of stress and strain in soils." *J. Soil Mech. Foundations Div.*, 96(5), 1629–1653.

Finno, R. J. and Calvello, M. 2005. "Supported excavations: Observational method and inverse modeling." *Journal of Geotechnical and Geoenvironmental Engineering*, 131(7), 826–836.

Fuentes, R., Pillai, A., and Ferreira, P. 2018. "Lessons learnt from a deep excavation for future application of the observational method." *Journal of Rock Mechanics and Geotechnical Engineering*, 10(3), 468 – 485.

Gelman, A. G., Roberts, G. O., and Gilks, W. R. 1996. "Efficient metropolis jumping rules." *Bayesian Statistics V*, 599–608.

Ghanem, R. G. and Spanos, P. D. 1991. *Stochastic Finite Elements: A Spectral Approach.* Springer, New York.

Haario, H., Saksman, E., and Tamminen, J. 2001. "An adaptive metropolis algorithm." *Bernoulli*, 7(2), 223–242.

Huang, J., Zheng, D., Li, D., Kelly, R., and Sloan, S. W. 2018. "Probabilistic characterization of 2D soil profile by integrating CPT with MASW data." *Canadian Geotechnical Journal*, doi:10.1139/cgj–2017–0429.

Jan, J. C., Hung, S.-L., Chi, S. Y., and Chern, J. C. 2002. “Neural network forecast model in deep excavation.” *Journal of Computing in Civil Engineering*, 16(1), 59–65.

Juang, C. and Zhang, J. 2017. “Bayesian methods for geotechnical applications-a practical guide.” *Geotechnical Safety and Reliability*, 215–246.

Juang, C. H., Luo, Z., Atamturktur, S., and Huang, H. 2013. “Bayesian updating of soil parameters for braced excavations using field observations.” *J. Geotech. Geoenviron. Eng.*, 139(3), 395–406.

Kung, G. T., Hsiao, E. C., Schuster, M., and Juang, C. H. 2007. “A neural network approach to estimating deflection of diaphragm walls caused by excavation in clays.” *Computers and Geotechnics*, 34(5), 385 – 396.

Lark, R. M. and Cullis, B. R. 2004. “Model-based analysis using REML for inference from systematically sampled data on soil.” *European Journal of Soil Science*, 55(4), 799–813.

Ledesma, A., Gens, A., and Alonso, E. E. 1996. “Parameter and variance estimation in geotechnical backanalysis using prior information.” *International Journal for Numerical and Analytical Methods in Geomechanics*, 20(2), 119–141.

Liu, W. F., Leung, Y. F., and Lo, M. K. 2017. “Integrated framework for characterization of spatial variability of geological profiles.” *Can. Geotech. J.*, 54(1), 47–58.

Lo, M. K. and Leung, Y. F. 2016. “Bayesian updating of subsurface spatial correlation through monitoring of infrastructure and building developments.” *Proceedings of the International Conference on Smart Infrastructure and Construction, 27-29 June 2016. Institution of Civil Engineers, London, UK*, 511–516.

Lo, M. K. and Leung, Y. F. 2017. “Probabilistic analyses of slopes and footings with spatially variable soils considering cross-correlation and conditioned random fields.” *J. Geotech. Geoenviron. Eng.*, 143(9), 04017044.

Lo, M. K. and Leung, Y. F. 2018. “Reliability assessment of slopes considering sampling influence and spatial variability by Sobol' sensitivity index." *J. Geotech. Geoenviron. Eng.*, 144(4), 04018010.

Minasny, B. and McBratney, A. B. 2005. "The Matérn function as a general model for soil variograms." *Geoderma*, 128(3-4), 192–207.

Najjar, S. S. and Gilbert, R. B. 2009. "Importance of lower-bound capacities in the design of deep foundations." *J. Geotech. Geoenviron. Eng.*, 135(7), 890–900.

Packham, N. and Schmidt, W. M. 2010. "Latin hypercube sampling with dependence and applications in finance." *Journal of Computational Finance*, 13(3), 81–111.

Papaioannou, I. and Straub, D. 2012. "Reliability updating in geotechnical engineering including spatial variability of soil." *Computers and Geotechnics*, 42, 44 – 51.

Peck, R. B. 1969. "Advantages and limitations of the observational method in applied soil mechanics." *Géotechnique*, 19(2), 171–187.

Phoon, K. K. and Kulhawy, F. H. 1999. "Characterization of geotechnical variability." *Can. Geotech. J.*, 36(4), 612–624.

Pickles, A. R., Lee, S. W., and Sun, R. Y. F. 2006. "Ground movement of deep excavation in reclamation." *Proc. Danube European Conf. on Geotechnical Engineering*, Vol. 2, 661–666.

Qi, X.-H. and Zhou, W.-H. 2017. "An efficient probabilistic back-analysis method for braced excavations using wall deflection data at multiple points." *Computers and Geotechnics*, 85, 186 – 198.

Sert, S., Luo, Z., Xiao, J., Gong, W., and Juang, C. H. 2016. "Probabilistic analysis of responses of cantilever wall-supported excavations in sands considering vertical spatial variability." *Computers and Geotechnics*, 75, 182 – 191.

Spross, J. and Johansson, F. 2017. "When is the observational method in geotechnical engineering favourable?." *Structural Safety*, 66, 17 – 26.

Wair, B. R., DeJong, J. T., and Shantz, T. 2012. *Guidelines for estimation of shear wave velocity profiles*. Pacific Earthquake Engineering Research Center.

Wang, Y., Au, S.-K., and Cao, Z. 2010. "Bayesian approach for probabilistic characterization of sand friction angles." *Engineering Geology*, 114(34), 354 – 363.

Wang, Y., Cao, Z., and Li, D. 2016. "Bayesian perspective on geotechnical variability and site characterization." *Engineering Geology*, 203, 117 – 125.

Wang, Y., Huang, K., and Cao, Z. 2014. "Bayesian identification of soil strata in London clay." *Géotechnique*, 64(3), 239–246.

Wu, S.-H., Ching, J., and Ou, C.-Y. 2014. "Probabilistic observational method for estimating wall displacements in excavations." *Canadian Geotechnical Journal*, 51(10), 1111–1122.

Yang, H.-Q., Zhang, L., and Li, D.-Q. 2018. "Efficient method for probabilistic estimation of spatially varied hydraulic properties in a soil slope based on field responses: A Bayesian approach." *Computers and Geotechnics*, doi:10.1016/j.compgeo.2017.11.012 (in press).

Yáñez-Godoy, H., Mokeddem, A., and Elachachi, S. M. 2017. "Influence of spatial variability of soil friction angle on sheet pile walls structural behaviour." *Georisk: Assessment and Management of Risk for Engineered Systems and Geohazards*, 11(4), 299–314.

Zhang, J., Tang, W. H., Zhang, L., and Huang, H. 2012. "Characterising geotechnical model uncertainty by hybrid Markov Chain Monte Carlo simulation." *Computers and Geotechnics*, 43, 26 – 36.

Zhang, J., Zhang, L. M., and Tang, W. H. 2009. "Bayesian framework for characterizing geotechnical model uncertainty." *J. Geotech. Geoenviron. Eng.*, 135(7), 932–940.